

# Multiscale dictionary of rat locomotion

Haozhe Shan<sup>1 2\*</sup>, Peggy Mason<sup>1</sup>

<sup>1</sup>Department of Neurobiology, the University of Chicago, Chicago, IL, USA. <sup>2</sup>Current address: Center for Brain Science, Harvard University, Cambridge, MA, USA. \* Corresponding Author.

## Abstract

To effectively connect activities and architecture of the nervous system to behavioral output, it is crucial to have a precise, accurate and complete description of stereotyped behavioral components (“motifs”) and how they are assembled to form observed behaviors. While some motifs have been uncovered and detailed in rats via human observation, discovering behavioral repertoires in this way is imprecise, slow and contaminated with biases and individual differences. As a replacement, we propose a framework for unbiased, efficient and precise mapping of rat locomotor activities. We propose that locomotion possesses multiscale structures – it is assembled from motifs of specific postures, movement of segments, and exploration patterns. We modeled the layered structure of behavior for the first time with multiple, parallel Markov chains that were obtained with hidden Markov models (HMM). We showed that even at minute-long timescale, observed behaviors are composed of motifs. In addition, the motifs are not only computationally distinct but biologically significant. We found that motif assembly is a heterogeneous Markov process. Finally, using layered computational models, we showed that motif assembly is strongly constrained to a few fixed behavioral “phrases”. The motifs potentially reflect outputs of canonical underlying neural circuits. Our approach and results for the first time capture behavioral dynamics at different spatial-temporal scales, painting a complete and detailed picture of how behaviors are organized.

## 1 Introduction

Intuitively, animal behaviors are produced at different scales, ranging from motor primitives to overarching strategies. For example, as a person has lunch, the motor primitives involve her placing the spoon on the plate and then in her mouth; on a larger scale, she returns to her office after she’s done eating. To adequately describe the behavior of lunch-having, one must be able to capture behavioral

motifs at multiple scales, transition structures between motifs at each scale, and mapping between motifs at different scales [35]. A more abstract representation of co-existing different behavioral scales is illustrated in Fig. 1.1 (b). The complexity of multiscale dynamics brings considerable inconveniences to behavioral neuroscience. Slow and large-scale dynamics are less apparent to human observers than fast, immediate ones, leading to slowly-evolving variations in fast dynamics that appear to be beyond deterministic explanation. Difficulties with describing behavioral dynamics are exacerbated by the field’s long-standing reliance on human observation and intuition to parse out individual, ethologically meaningful segments of behavior. These segments are sometimes poorly aligned with their supposed ethological meaning.

The lack of precise, complete and coherent description of animal behavioral dynamics has far-reaching consequences on biological sciences. Consider rats, one of the most commonly used model organisms across fields. In many investigations, especially those interested in behaviors and their neural substrates (e.g. neuroscience, psychopharmacology), stereotyped behaviors of rats are used as critical measurements. Noted applications of rat behavioral measurement include the open field (OF) test and the elevated plus maze (EPM) for anxiety-like behaviors, forced swimming test for depression-like behaviors, the Von Frey assay for mechanical nociceptive sensitivity and so on [11, ?, 17, 31, 33]. Behavioral assays of rats are well-established components of rodent models of neural functions and psychiatric conditions from spatial memory and empathy to autism spectrum disorder and major depression [2, 16, 20, 24]. Due to the feasibility of large-scale, automated data collection (via tracking systems, for example), locomotion is the most frequently analyzed behavior. Locomotion is also part of virtually any behavioral assay. In addition, stereotyped behaviors have also been defined and used in behavioral assays. The link between a stereotyped behavior and its ethological meaning, such as boxing and lateral threat for social aggression[8], thigmotaxis for anxiety[29], and licking and grooming for maternal care[23], are proposed based on human intuition, derived from observing rat behaviors, and detected by human observers using often imprecise definitions. While existing movement-to-meaning connections have validity, additional meaningful locomotive patterns that can be readily discovered by an unbiased algorithm are likely to exist.

Relying on convention and intuition for experimental analysis leads to limited possibilities and an inaccurate represen-

tation of the reality. To illustrate one common limitation, the EPM, considered to be a specific test for anxiety-like states, has an injective but not bijective relationship with anxiety analogs. In other words, variations in EPM read-outs may reflect hidden states other than anxiety. Behavioral metrics are vulnerable to variations in experimental setup, and sometimes these variations have interactions with the hidden states of interest. For example, metrics reflecting anxiety-like behaviors in the Elevated Plus Maze test are sensitive to rats' prior experience with human handling and the illumination of the test room. These factors selectively sensitize rats to some anxiolytic treatments but not others[?]. Finally, in locomotion analyses the exact definitions are often based on arbitrary hunches. For instance, it is well known that thigmotaxis, rodents' preference to be located near the boundaries of testing environments, is an index of anxiety[29]. However, how much of the area around the boundaries should be defined as peripheral? Such questions are currently answered arbitrarily.

Without systematic investigations and adequate knowledge of the repertoire and dynamics of rat behaviors, what human coders define as "stereotyped behaviors" can be poorly aligned with actual repeated and meaningful behavioral motifs in the animals; the behavioral markers that human observers have associated with hidden states of interest may not be the most precise or accurate. Understanding animal behaviors with this approach is akin to understanding a foreign language with no knowledge of either its vocabulary or grammatical structures. Being able to parse out what are the real stereotyped motifs ("vocabulary"), and how they are organized and assembled into observed behavioral sequences ("syntax"), will greatly aid efforts to understand the meanings of behaviors. This calls for an assumption-free, unbiased identification approach.

There have been some successful attempts to use fully unsupervised, unbiased mathematical models to map out behavioral repertoires in animals[6, 9, 34]. In these efforts, distinguishable and stereotyped motifs are identified from behavioral output computationally, seeding identification of behavioral repertoires. Yet, such approaches to date have ignored the multi-scale embedding structure of behavioral motifs. Importantly, as evident from Fig. 1.1 (b), the geometry of large-scale motifs cannot be described by the assembly principles of small-scale motifs. Thus, the single-scale modeling approach that is prevalent in animal behavioral modeling cannot capture the full repertoire of behaviors, particularly the larger-scale ones. In addition, some of the previous mathematical models of behaviors use straightforward clustering algorithms (e.g. K-means, see [14]), which overlook transition dynamics between motifs.

We propose a new computational approach that, for the first time, reveals the existence, geometry and transition dynamics of rat behavioral trajectories at *multiple timescales*. In terms of model design, we combined hidden Markov modeling (HMM) with a segmentation-decomposition procedure,

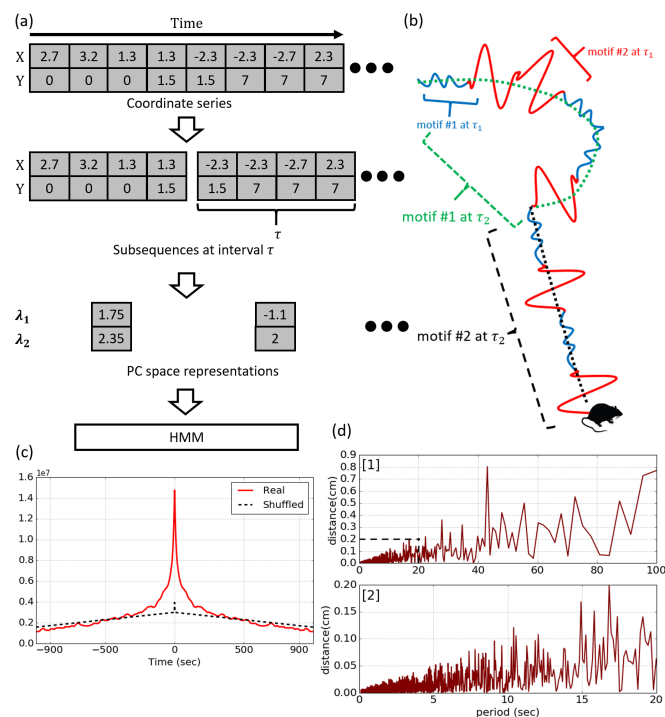


Figure 1.1: Multi-scale structure of locomotor trajectory motifs calls for a segmentation-decomposition procedure. (a) The segmentation-decomposition procedure. Granularity was forced at interval  $\tau$  onto HMMs by segmenting the data series first and decomposing them using principle component analysis. (b) Motifs in rat locomotor trajectories exist in parallel on different spatial-temporal scales. Fully describing the trajectory illustrated here, for instance, requires mapping of the geometry of lower and higher timescale motifs, as well as the assembly rules at two different scales. Their linear representations in the PC space (shown here in the third step) are fed into HMMs. (c) Autocorrelation function of locomotor data. (d) Period spectrum (period being the reciprocal of frequency) from Fourier decomposition of locomotor trajectories. [2] is a blown-up view of parts of [1].

which forced predetermined, explicit constraints on the spatial scales of motifs and the temporal scales of dynamics. The result is a model that views behavioral trajectories as the outcome of multiple Markov processes organized hierarchically based on their respective scales. We tested the validity of this view, as well as the experimental significance of the discovered motifs. Our approach shows the limitations of traditional single-scale modeling and identification of behavioral sequences. Our results motivate a new, multi-scale perspective on animal behavior modeling.

## 2 Materials and Methods

### 2.1 Experimental set-up

The basic paradigm for the experiments has been described in detail before [2, 3, 4, 28]. In the behavioral experiments, an adult male Sprague-Dawley (SD) rat was placed into a custom-built Plexiglas restrainer individually. Restrainers have a door on only one side that can only be opened from the outside through physical action (no electronic buttons/levers etc.). Each restrainer is placed in the center of a 50-by-50 cm arena, walled off with Plexiglas panels. The rat in the restrainer is hereby referred to as the “trapped rat”. In each arena, another adult male SD rat of similar age and size was placed outside of the restrainer. Rats that were allowed to move freely in the arenas are hereby referred to as “free rats”. In each experimental “session”, the restrainer and the trapped rat were placed in the center of the arena and the free rat was introduced to the arena; if the free rat did not open the restrainer and release the trapped rat within 40 minutes, an experimenter propped the door half-open 40 minutes after the session had started; the free rat was then given 20 minutes in the arena. If the free rat opened the door at any point, the session continued until an hour was up. Therefore all sessions lasted for an hour. Each free rat was tested for one session per day for 12 days.

### 2.2 Data collection

In the particular dataset used here, a total of 24 free rats and 24 trapped rats were tested for 288 sessions (12 for each pair of free rat and trapped rat). Only the first seven days of sessions were analyzed ( $N=168$ ). Moreover, the same 16 free rats received an intraperitoneal (i.p.) injection of nadolol 15 minutes before each session and the remaining 8 free rats received an i.p. injection of propranolol. The injections took place before all the sessions. Trapped rats received no injections. Originally the data were collected to test the effects of propranolol and nadolol treatment on prosocial behaviors in rats. The nadolol data were previously reported in [4].

During behavioral testing, a wide-angle CCD camera was placed above each arena, fastened with a custom-built

camera holder for stability. All behavioral sessions were videotaped thusly. After behavioral testing had finished, the videos were analyzed off-line using the EthoVision software[22]. The software allows automated video-based tracking of the subjects in the arenas throughout the session. To allow the software to distinguish the trapped rat and the free rat in each session, the rats were marked with markers of different colors during testing. Tracking was performed at 15 frames per second, generating a 2-tuple coordinate (X-Y) for each frame. No further analysis was performed in the software, and the raw tracking data were exported for further analysis. The raw data for each session were therefore a two-dimensional time series that spans across 60 minutes at 15 frames per second ( $\sim 54,000$  tuples of coordinates). Since rats were being placed into the arenas in the first 5 minutes of the session, and the last 20 minutes of each session involves a half-open restrainer door instead of the standard closed door, they were not included in any analysis.

The 24 free rats were tested for 12 sessions, each with 35 minutes of tracking at 15 frames per second, resulting in  $\sim 9$  million tuples of coordinates.

### 2.3 Analysis outline

The main aim of the current analysis is to discover stereotyped, repeated motifs in behavioral (specifically, locomotor) trajectories, and identify the rules that govern their assembly into the observed locomotive behaviors. The complete locomotive trajectories were first segmented at different timescales, resulting in short trajectory segments at various levels of granularity. Next, linear dimensionality reduction was performed on the segments with principle component analysis (PCA), representing each segment in a 5-dimensional principle component space. We then obtained low-dimensional representations of the segments, and determined the order of their assembly in complete trajectories. We investigated whether there exist stereotyped, repeated segments (which we term “motifs”), and whether they are assembled according to certain rules by fitting hidden Markov models (HMM). Assumptions about motifs and their transition dynamics were tested by comparing HMMs against mixture models. We then tested whether the motif assembly satisfies the assumption of Markov property by examining two statistical signatures. We found that HMMs are appropriate models for identifying motifs and their assembly rules in rat locomotor data, and went on to perform other analyses using the motifs and rules identified by HMMs. A step-by-step description of these analyses is offered below.

## 2.4 Multi-timescale feature extraction

### 2.4.1 Multi-timescale feature extraction through lateral decomposition

A valuable step to reduce the dimensionality of locomotor data is to discover high-dimensional stereotyped patterns, which in turn can be used to reconstruct original locomotor sequences combinatorially. A frequently used approach in similar dimensionality reduction problems (e.g. speech recognition, motion recognition) is to discover instantaneous motifs (i.e. duration of one frame) that can be sequentially combined to form locomotion trajectories. This approach may be favorable for cases where each frame has a high degree of freedom, such as when modeling pose trajectories[34]. However, locomotor data at each frame has a very low degree of freedom. Therefore, modeling locomotor data in this way is unlikely to capture trajectories of interest. There are extended versions of the HMM, such as the Autoregressive Hidden Markov Model, ARHMM, and the Hierarchical Hidden Markov Model, HHMM, that include some slower dynamics by either expanding the transition matrix to include motifs further back in time (in the case of ARHMM, see [32]) or adding “meta-motifs” each of which has its own transition matrix of motifs (in the case of HHMM). However, they make constraining assumptions about the structure of the meta-motifs and are therefore ill-suited for multi-timescale motif discovery[1].

We employed a different approach that we term the “segmentation-decomposition” procedure. It relies on lateral decomposition of locomotor trajectories (e.g., each sequence is the weighted sum of several “eigensequences”), instead of a sequential combination as outlined above. A key difference between the two approaches is that while sequential addition of motifs can use motifs of the same length to recover meaningful behavioral structures of different lengths (by fitting a transition probability matrix, for instance), lateral additive combination requires the length of the locomotion segments to be predetermined. In other words, the locomotion trajectories must be segmented first, and decomposed second. A diagram illustrating the procedure is offered in Fig. 1.1 (b).

Determining the temporal-spatial scales of motifs in locomotor data is a central problem when parsing animal behavior data into meaningful segments (for discussion and solutions of this issue in non-rat organisms, see [6, 9, 34]). In our case, there are two scales of interest – the timescale of motif assembly (e.g. how long is each motif used before it transits into a different motif?), and the spatial scale of motif geometry (the spatial-temporal scale of each motif). Temporal and spatial scales are related by constraints of rats’ velocity. In addition, motifs may exist at multiple scales simultaneously (as is assumed here), further complicating scale selection. Mitigating the problem is the fact that the timescales of segmentation selected here do not dictate the timescale of data structures (e.g. one-second segmentation can reveal five-second structures via specific transition structures).

In the current analysis, the trajectories were segmented at 1, 5, 10, 15, 30, and 60 second intervals. While these selections are somewhat arbitrary, note that segments created at each interval contain information about slower dynamics in the assembly rules. The manual selection of these intervals was guided by a few analyses. First, the autocorrelation of locomotor data drops below the level of permuted data at around 300 seconds (Fig. 1.1(c)). This creates an upper bound for the timescale of structured locomotor trajectories. Second, the period spectrum, constructed with the Fourier transform of locomotor data (Fig. 1.1 (d)), shows a linearly increasing amplitude across periods. We hereby denote the length of segmentation as  $\tau$ .

Once created, the segments of locomotor trajectories were rotated and displaced to always start from the origin and in the direction of the Y-axis. Separate principle component analyses (PCA) were then performed on the resulting segments to extract principle components of different scales. Surprisingly, the PCAs showed that the segments at different timescales could be efficiently decomposed into only a few eigen-trajectories. While this is less unexpected for the 2-second timescale, where each segment is merely 60-dimensional, it is unusual that segments taken at longer timescales (e.g. 30 seconds, where they are 900-dimensional) could also be decomposed efficiently. In all timescales analyzed, the first five principle components could explain over 85% of the total variance. The first two principle components are dominant across timescales, accounting for 70% of the variance. These results reveal highly manifolded structure in locomotor trajectories, paving the road for further analyses. Eigen-trajectories and percent variance explained are shown in Supplementary Materials.

## 2.5 Unbiased motif discovery with Gaussian Hidden Markov Models

The PCA of segments of different sizes ( $\tau$ ) represents a dramatic dimensionality reduction of the high-dimensional locomotor trajectories. This is especially true for larger timescales (e.g. at 30 seconds, the 900-dimensional segment is represented in a 5-dimensional principle component space). This allows efficient modeling of rat behaviors at supra-second timescales. To determine if there are stereotypical segments (i.e. motifs) and non-trivial transition dynamics between such motifs, Gaussian-emission hidden Markov models (HMM) were fitted to segments in the principle component space.

The structure of the model can be summarized as follows. The segments are represented as vectors in the 5-dimensional principle component space (“PC space”). The model attempts to discover clusters in the principle component space, each of which may be a stereotypical behavioral motif that the rat reuses. Each behavioral motif is represented as a multivariate Gaussian distribution, specified with means and a covariance matrix between dimensions in the PC

space. Since the model also has access to the sequential structure of these motifs, it infers the transition probability matrix between the motifs. In other words, for  $N$  sequential observations in a  $D$ -dimensional space with  $K$  motifs ( $K$  is manually entered as a parameter), the model generates and fits an  $N$ -by- $N$  transition probability matrix ( $\mathbf{A}$ ),  $K$  multivariate Gaussian distributions, each with a mean vector  $\boldsymbol{\mu}$  of size  $D$  and a  $D$ -by- $D$  covariance matrix ( $\boldsymbol{\Sigma}$ ), and the probabilities of the motifs for the first observation, specified by a vector of size  $K$  ( $\boldsymbol{\Pi}$ ). The implicit hypotheses of HMM are therefore that there exist  $K$  stereotypical behavioral motifs, and that they have a Markovian transition structure. Another notation of use is a state vector  $\mathbf{S}$  of size  $N$ , which represents which motif is employed at different time points. We use  $S_t \in \{0, 1, 2, \dots, K\}$  to denote which motif is used at timepoint  $t$ . The model is fitted with the forward-backward algorithm[5], embedded in the expectation-maximization (EM) algorithm[19]. After the model had been fitted, Viterbi algorithm[12] found the motifs most likely for each behavioral segment. Parameters of the model were initialized by performing K-means clustering on the data. [7] offers a detailed look at implementations of these algorithms. A discussion of HMMs is offered in Supplementary Materials.

Null hypotheses can be tested by fitting the data with alternative models and performing model selection. To test the hypothesis that transition probabilities are dependent on the current behavioral motif, we fitted a Gaussian Mixture Model (GMM) with  $K$  components onto the data. Like the HMM, GMM assumes the existence of  $K$  motifs, each represented by a multivariate Gaussian distribution. However, while in the HMM  $p(S_{t+1})$  is conditioned on  $S_t$  (as specified by the transition matrix),  $p(S_{t+1})$  is time-invariant in GMMs. In other words, motif selection in a GMM is stochastically drawn from a fixed probability distribution. To test the hypothesis that there are multiple stereotypical behavioral motifs, we fitted the data with a special case of GMM where  $K = 1$  (which we simply refer to as the Gaussian model, or GM, since there’s no “mixture”). This model assumes that all observed vectors in the PC space can be explained by a single multivariate Gaussian probability distribution.

The three competing models (HMM, GMM, GM) were compared by judging how well they fit randomly selected held-out locomotion trajectories, using maximized likelihood as a measure.

## 2.6 Discovering cross-timescale hierarchies with Layered Hidden Markov Models

To recap, to extract patterns of different timescales, we performed principle component analysis of trajectory segments sampled from the locomotion trajectories at different lengths, and then fitted individual HMMs for the decomposed version of these segments in the principle component

space. However, this approach parses behavioral motifs at different timescales independently and does not propose a projection from lower-timescale motifs to higher-timescale motifs, which would offer insight into how long-term motifs are supported and exhibited in the short term.

A natural model structure for this purpose is layered hidden Markov model (LHMM). LHMMs are widely used in machine learning to extract higher-order hidden states (e.g. intent in motor actions, phonemes in speech recognition) from lower-order observations (e.g. movement trajectories and auditory recordings [10, 21, 30]). Conceptually, LHMMs posit that the hidden states in the data may have a hierarchical structure - lower level hidden states, such as movement motifs, may give rise to higher-order hidden states, such as motor intentions. More formally, in an LHMM, several independently fitted HMMs are layered on top of each other, with the output of the lower layer passed onto the next layer as input. In its most basic form, if we denote the HMM at layer  $l$  as  $HMM_l$ , which is specified by a set of parameters  $\{\mathbf{A}_l, \boldsymbol{\pi}_l, \boldsymbol{\mu}_l, \boldsymbol{\Sigma}_l\}$ , fitted on input vectors  $\mathbf{O}_l$  and gives an output vector of labels  $\mathbf{K}_l$ , then we have

$$l \in [1, L] : \mathbf{O}_l = \mathbf{K}_{l-1}.$$

and the lowest-level HMM is directly fitted onto the observations themselves.

An important modification to the standard LHMM made in the current study is that instead of merely the labels, which represent a winner-take-all strategy for the competing behavioral motifs, lower-level HMMs pass the means of each modes as observation symbols to higher levels. Formally,

$$l \in [1, L] : \mathbf{O}_l = \boldsymbol{\mu}_{l-1}.$$

Both higher layers of the LHMM and HMM fitted to segments created at long intervals extract large-timescale patterns, but there is a crucial difference in our particular application. Recall that the segments were translated to start at the origin and rotated to initially traverse along the Y axis. For the HMM, this means that the long-interval segments tend to end further away from the origin, and a large component of the variance comes from displacement; however, since lower-layer models in the LHMM take in shorter segments, which are all displaced and rotated, displacement is reduced as a source of variance. Therefore, using parallel HMMs allows discovery of the geometry of high-timescale motifs, while LHMM informs of the assembly rules of low-timescale motifs.

### 3 Results

#### 3.1 Rat locomotion is composed of distinct motifs across scales

At the timescales considered in the current analysis (1 sec to 60 sec), HMMs and GMMs (both of which assume more than one stereotyped motifs) are favored over GM, which assumes a single motif. To determine how many behavioral motifs exist at each timescale, multiple HMMs and GMMs with different values for  $K$  were fitted over data and  $K$  with the highest likelihood was selected. Models were tested on randomly selected held-out data (30% of entire dataset) to generate the statistics for model comparison. It is important to note that since best-fit likelihood is a function of sample size[15], we standardized the sample size to the mean length of a behavioral session for the purpose of model selection. Nevertheless, across the timescales analyzed in the current study, HMMs and GMMs outperformed their GM counterpart, supporting the existence of discrete, stereotyped behavioral motifs. HMMs also consistently outperformed GMMs, supporting the existence of non-uniform transition structures at these timescales (Fig. 3.1, top panels). Since the model is tested on held-out data, model likelihood does not monotonically increase as a function of  $K$ . Therefore, the best fitting HMM is selected to be the one with the highest likelihood (Fig. 3.1, bottom panel).

Motifs can be reconstructed by linearly combining principle components. We reconstructed the most common 3 motifs at each timescale. They are shown in Fig. 3.2.

#### 3.2 Motifs assembly rules are Markovian

A stochastic process is said to possess the Markov property if the probability distributions of states at the next time point are conditioned upon the state at the current time point and only the current time point[27]. In the context of behaviors, this essential means that the selection of the next motif depends and only depends on what motif is being used currently. For instance, if the rat is alternating between walking and sniffing consistently, then the process likely possesses the Markov property. Formally, we can write

$$p(S_{t+1}|S_t) = p(S_{t+1}|S_t, S_{t-1}, \dots, S_1).$$

Modeling with HMMs explicitly assumes that transition between locomotive motifs is Markovian. Hence, it is worthwhile to test whether this is true. Markov property can be violated in two ways. The first possibility is that motif selection has no history dependence at all (i.e.,  $p(S_{t+1}|S_t) = p(S_{t+1})$ ). To see whether this is true, note that if  $p(S_{t+1})$  is conditioned upon  $S_t$ , then one would expect a non-zero mutual information between the random variables  $S_{t+1}$  and  $S_t$ . Therefore, whether the generative process has history

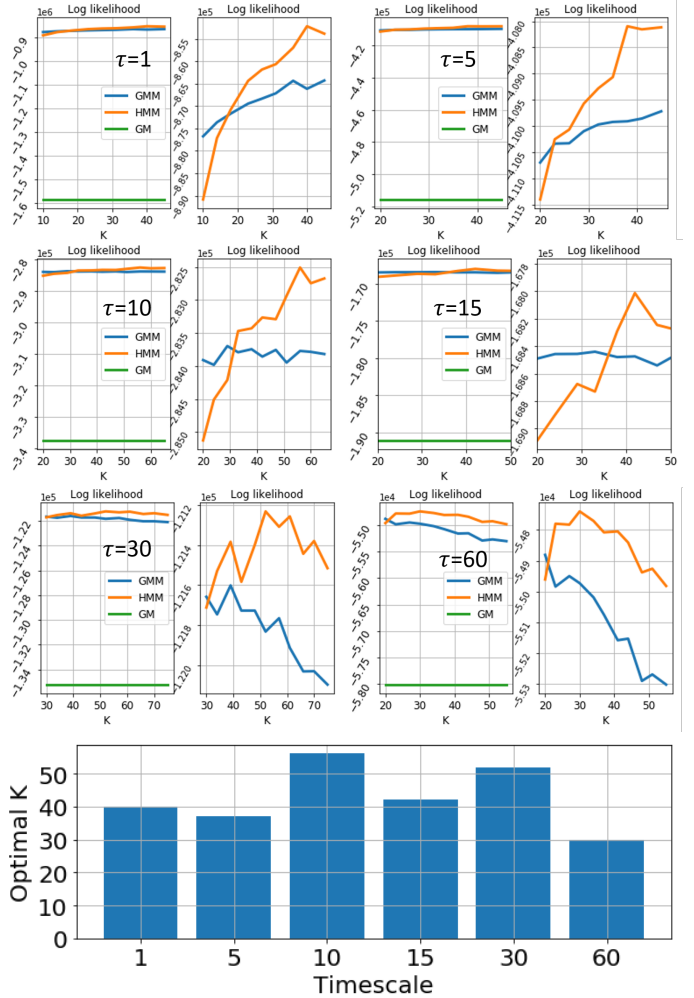


Figure 3.1: Model comparison consistently favors HMMs across timescales, suggesting stereotyped motifs and transition structure. Top panel: log likelihood-based evaluation of Gaussian mixture models (GMM), hidden Markov model (HMM) and Gaussian model (GM) on held-out dataset. Bottom panel: Best fitting  $K$  across timescales.



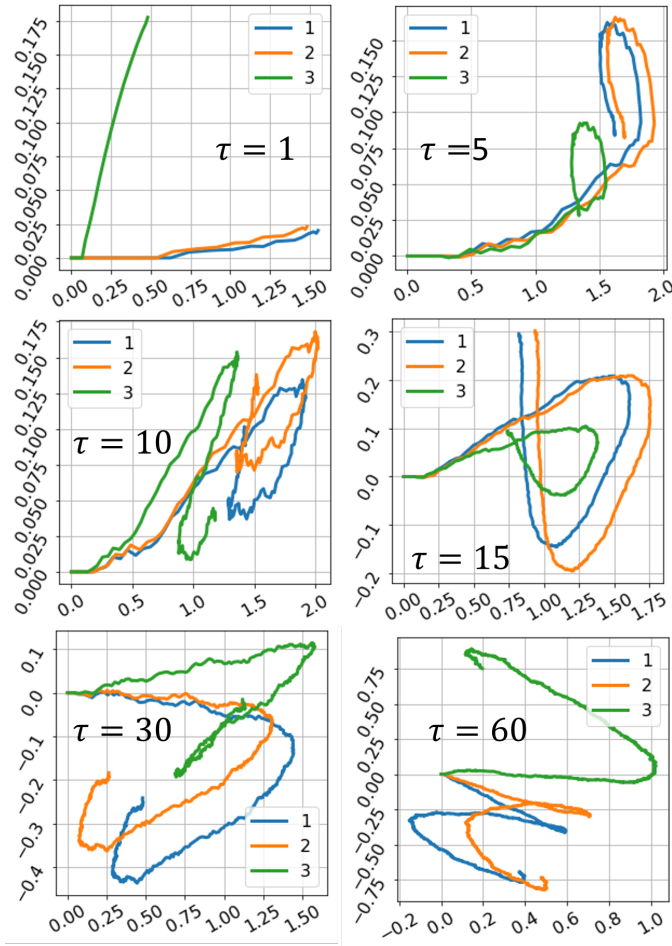


Figure 3.2: Most common 3 motifs at each timescale were reconstructed through linear recombination. X-Y dimensions describe the arena floor. Unit in centimeters.

dependence can be determined by computing the mutual information between consecutive motifs in the HMMs. Note that using mutual information instead of autocorrelation as measurement allows non-converging transition dynamics to be included. To compute the mutual information, we use [18]:

$$MI(S_{t+1}; S_t) = \sum_k^K \sum_j^K p(S_{t+1} = k, S_t = j) \log \frac{p(S_{t+1}=k, S_t=j)}{p(S_{t+1}=k)p(S_t=j)}. \quad (3.1)$$

Since  $p(S_{t+1} = k, S_t = j) = p(S_{t+1} = k, |S_t = j)p(S_t = j)$ , the first term of which is specified by the transition matrix, all one needs is to estimate the marginal probabilities. Note that since all the transition matrices fitted are positive recurrent, they are bound to converge. Therefore, the marginal probabilities are dependent on how long the Markov process is allowed to run. To estimate the mutual information within realistic experimental timescale, we thus simply estimated them empirically by observing the frequency of motif usage in the data analyzed. Finally, to see how history dependence is a function of jump size (i.e. how far apart two motifs are in time), we computed the mutual information at different jump sizes (Fig. 3.3 (a)). Note that a shuffled motif sequence analytically has zero mutual information between any two motifs. Therefore, the non-zero mutual information between adjacent motifs signals history dependence.

Another possible violation of Markov property is that the generative process has history dependence beyond the immediately previous motif. To test this possibility, we simply saw if the Chapman-Kolmogorov equation holds[13]. In our particular case, the equation states that

$$p(S_t|S_{t-a}) = \sum p(S_t|S_{t-b})p(S_{t-b}|S_{t-a})dS_{t-a} \quad a > b > 0. \quad (3.2)$$

Multiplying both sides of eq.(3.2) with  $p(S_{t-a})$ , it is equivalent to the easier-to-verify

$$p(S_t, S_{t-a}) = \mathbf{T}^a S_{t-a}, \quad (3.3)$$

where  $\mathbf{T}$  is the transition matrix. The disagreement between both sides of eq.(3.2) was quantified by computing the Kullback-Leibler divergence between the two distributions. The divergence was computed at different jump sizes. The results are shown in Fig. 3.3 (b). It can also be quantified by the maximum prediction accuracy of incidences of actual transitions using computed joint probability distributions. Equivalently, we computed the minimum Hamming loss of predictions at different timescales and different jump sizes. Results are shown in Fig. 3.3 (c). For this computation, a lower bound for Hamming loss given the complete marginal distribution of true motifs and distribution of motifs was first derived (an informal proof is offered in Supplementary Materials). The bound states

$$\mathcal{L}^H(\mathcal{S}, \hat{\mathcal{S}}) \geq \frac{1}{2} \sum_{k,j} |p(S_t, S_{t-a}) - \mathbf{T}^a S_{t-a}|.$$

Analysis using both metrics suggests that the Markov property is more valid with larger-timescale motifs, as the two sides of the Chapman-Kolmogorov equations have less disagreement. Implication of deviations from Markov property is discussed below.

### 3.3 Long-timescale history dependence

Figure 3.3 shows that there are failures of Markov property in the observed data, especially at lower timescales. In other words, while motif selection is largely dependent on what motif was being used previously, it also depends on motifs used further in the past. To investigate whether the failures are random or structured and what the non-Markovian history dependence is, we analyzed another important signature of Markov property – memorylessness. The duration of each motif in a memoryless process should obey a probability density function (pdf) that exponentially decays across time. We therefore computed the pdfs of different motifs and simply fitted exponential functions to them.

Remarkably, the pdfs are fitted almost perfectly with exponential functions (Fig. 3.4). For motifs of sizes of 1 second and 5 seconds, coefficient of determination ( $r^2$ ) of fitting the duration pdfs with exponential functions (in the form of  $y = ae^{bt} + c$ , where  $a, b, c$  are parameters) are well above 0.99 (1 sec,  $\bar{r}^2 = 0.997, \tilde{r}^2 = 0.999$ ; 5 secs,  $\bar{r}^2 = 0.997, \tilde{r}^2 = 1.000$ ). To ensure that the apparent memorylessness is not an artifact of transition structure assumptions in hidden Markov models, we performed analogous analysis on motifs labeled by Gaussian mixture models at 1 sec and found similar levels of goodness-of-fit ( $\bar{r}^2_{GMM} = 0.997, \tilde{r}^2_{GMM} = 1.000$ ; 5 secs,  $\bar{r}^2_{GMM} = 0.994, \tilde{r}^2_{GMM} = 0.999$ ). The analysis was repeated to see if memorylessness is a property of the generative process at different timescales, and exponential functions were reliably good fits for the duration pdfs (Fig. 3.4). This shows that features of rat locomotion behaviors at different timescales are generated by memoryless processes.

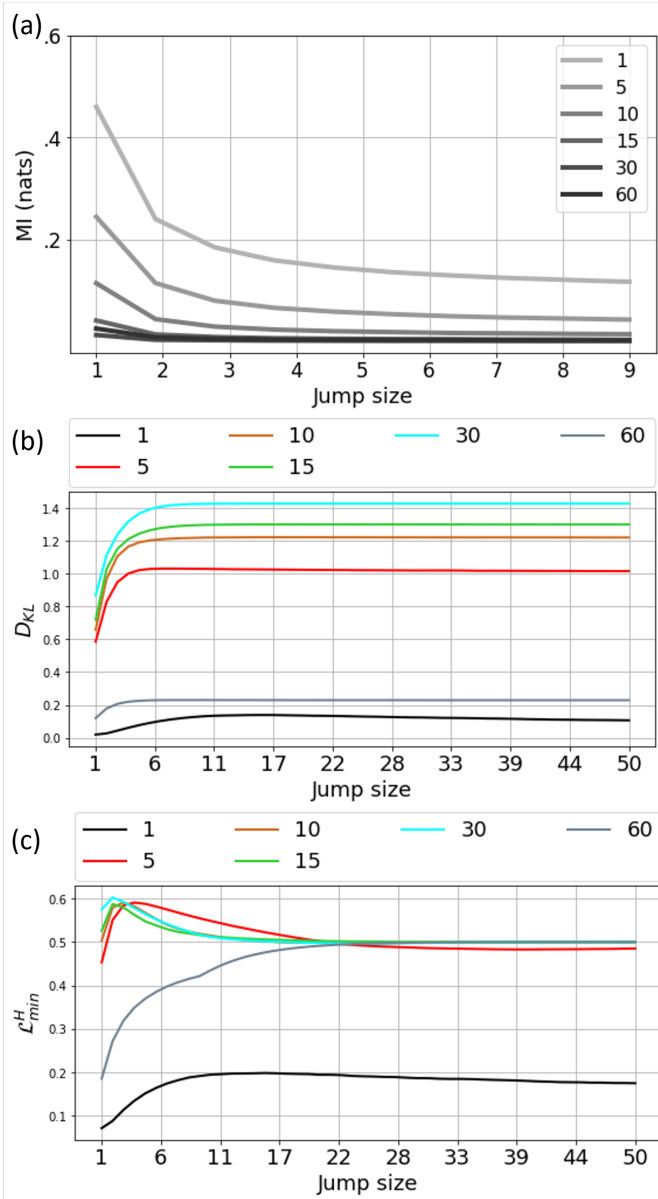


Figure 3.3: Statistical tests for Markov property in motif transition. (a) Mutual information between adjacent motifs decreases with increasing timescale and increasing jump size. (b) Deviation from Chapman-Kolmogorov equation, measured in Kullback-Leibler Divergence ( $D_{KL}$ ). (c) Same deviation as (b), measured in maximum prediction accuracy (minimum Hamming loss).

### 3.4 Spatial-temporal context influences motif assembly

So far it has been established that the the assembly of motifs into locomotor trajectories have deviations from the Chapman-Kolmogorov equation, pointing to potential non-Markovian history dependence, and yet the processes are strictly memoryless, since motif duration follows exponentially decaying probability distributions. These findings paint an interesting picture for motif selection policies in the rats. A plausible process that is consistent with both findings is a heterogeneous Markov process (e.g. the transition



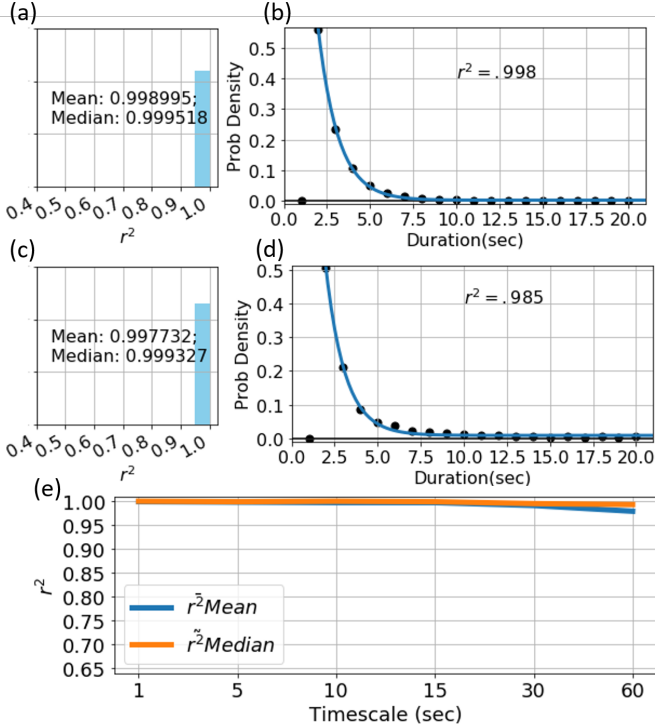


Figure 3.4: Coefficient of determination ( $r^2$ ) of fitting duration pdfs with exponential functions. (a) Histogram of  $r^2$  from exponential function fitting across motifs at  $\tau = 1$ . (b) An example showing exponential function fitting of one motif at  $\tau = 1$ . (c) Histogram of  $r^2$  from exponential function fitting across motifs at  $\tau = 5$ . (d) An example showing exponential function fitting of one motif at  $\tau = 5$ . (e) Statistics of  $r^2$  across timescales.

rules between motifs change over time). The heterogeneity could be due to either noise, or more interestingly, inherent heterogeneity in motif selection policies. Here, we test the hypothesis that heterogeneity is responsible for the apparent deviations from Markov property.

### 3.4.1 Existence of heterogeneity

Behavioral motif usage and transition are subject to several constraints that are not homogeneous across time-space. The local physical environment, for example, is not boundless and has inconsistencies within it - in our particular set up, the center of the arena features a restrainer with a trapped conspecific. In addition, latent states such as anxiety or physical energy expenditure may not be uniform across space-time. Therefore, while over all the sessions the models fitted  $K$  motifs, at each point in space-time only a subset of them ( $K_{sub}$ ) are available. This in turn constrains the transition structure - the full  $K$ -by- $K$  transition structure gives way to a  $K_{sub}$ -by- $K_{sub}$  transition structure. In other words, temporal-spatial heterogeneity of the generative process of locomotion trajectories constrains marginal and conditional probabilities, making them functions of space-time. In the parlance of hidden state modeling, there are additional high order hidden variables (space-time, which is not available in the trajectory segments and therefore hidden) that account for transition structures in first-order hidden variables (behavioral motifs).

Such heterogeneity can be straightforwardly shown by investigating if the marginal and conditional probabilities are functions of space-time by computing them at different points in space-time. In terms of space, the arena floor is divided into a 15-by-15 grid. The results are shown in Fig. 3.5 (a). We can similarly compute the observed joint probability distribution  $p(S_{t+1}, S_t)$  using this approach (Fig. 3.5(b)). For ease of illustration, we show the means and standard deviations of the marginal probabilities (i.e. motif usage probabilities) across the spatial grid; for joint probabilities (i.e. first-order transition probabilities), we show the entropy of the probability distribution of each transition across the grid. Results suggest that, as one would expect, rat locomotion has strong spatial heterogeneity. However, it is worth noting that the variability demonstrated here is not simply the variability of traces (e.g., U-turns are more common at edges than at the center), but variability of behavioral motifs (e.g. gait, posture, locomotion strategies).

### 3.4.2 Structure of heterogeneity

Once the models have been fitted, parameter sets that describe the motifs are fixed. From here, labeling each segment with a motif, given the motif parameters ( $\mu, \Sigma$ ) and the transition probabilities ( $\mathbf{A}$ ), becomes a high-order multi-label classification problem. Directly, the model labels each

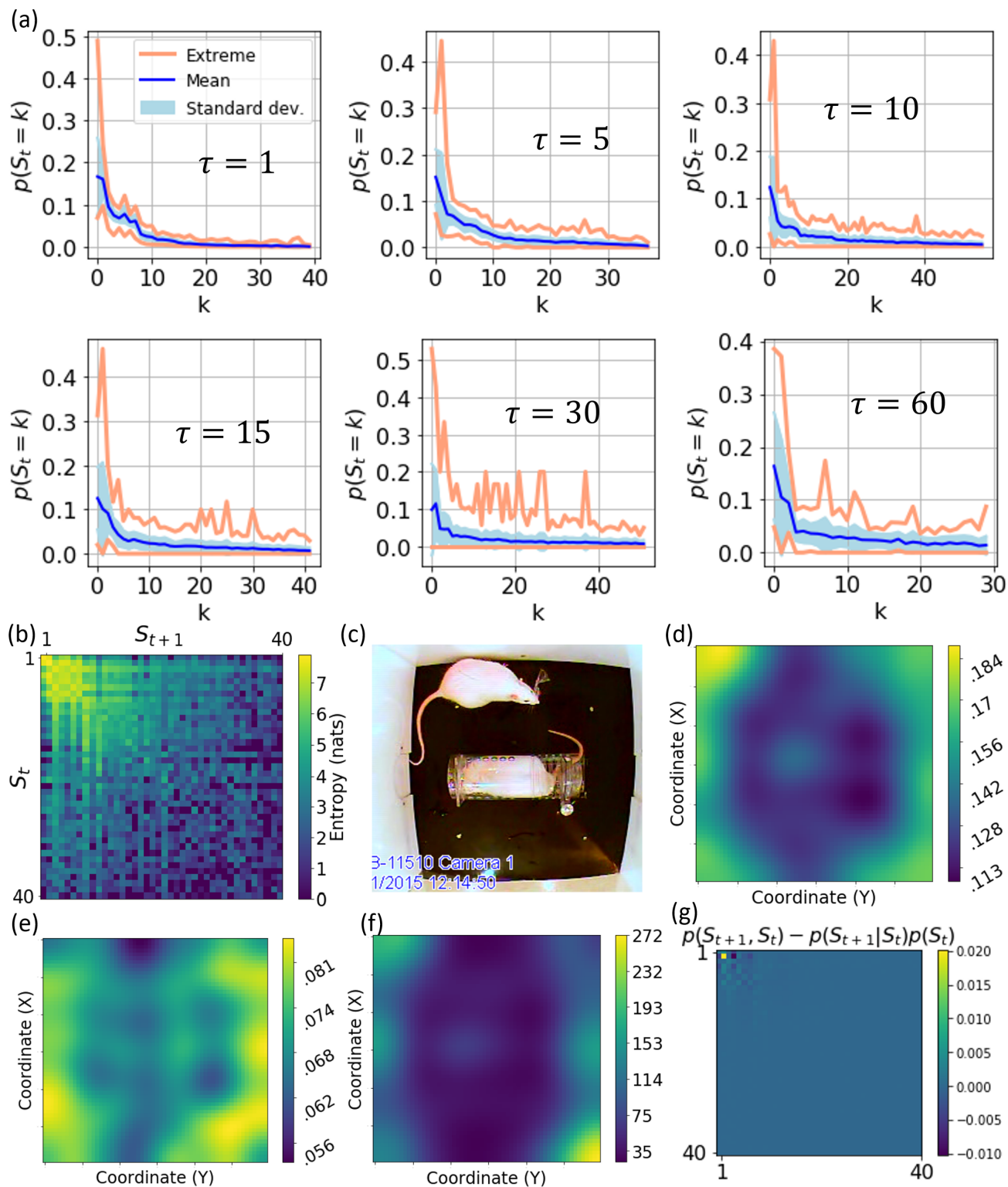


Figure 3.5: Transition probabilities and marginal probabilities show variability across space. (a) Variability of 1, 5, 10, 15, 30, 60-sec motifs across space. (b) Entropy of probability distributions of possible transitions over space. ( $\tau = 1$ ) (c) Image showing the physical landscape of arenas. (d) Heatmap of motif #2 usage across space showing spatial structure of transition heterogeneity. Heatmaps use 60-by-60 bins and 2-dimensional Gaussian filters for smoothing ( $\sigma = 5$ ) (e) Motif #2 Self-transition probability. (f) Overall placement of subjects across space. (g) Prediction of first-order transition has structured errors. Error is calculated as computed distribution minus observed distribution.

segment with a label  $S_t$ , the correct answer of which cannot be accessed; however, on higher orders, the model labels transitions (e.g. label adjacent segments with  $S_t, S_{t+1}$ ) in two ways. In the approach taken previously, given the parameter set of the model  $\{\mathbf{A}, \boldsymbol{\pi}, \boldsymbol{\mu}, \boldsymbol{\Sigma}\}$  we used the Viterbi algorithm to find the most likely sequence of labels that explain the data. We thus obtained a sequence of labels from which first-order transitions (or higher) can be found. The probability distribution of second-order transitions (i.e. the joint distribution  $p(S_t, S_{t+1})$ ) can be thus computed from the “observed” sequence of labels. Alternatively, this joint distribution can be computed using the observed marginal distributions of motifs ( $p(S_t)$ ) and the transition matrix (e.g. the conditional,  $p(S_t + 1|S_t)$ ). If the transition matrix perfectly captures the transition dynamics in the generative process, then given a long enough sequence of segments, where the probability distributions are fully explored, one should expect:

$$N \rightarrow \infty : p(S_t, S_{t+1})_{observed} = p(S_t + 1|S_t)p(S_t).$$

However, if the transition dynamics are not homogeneous in the generative process, fitting it with a fixed transition matrix creates inevitable prediction errors. Here we focus on first-order transition (jump size of one) and observe the structure of the error by simply comparing the observed and computed probability distributions (Fig. 3.5 (g)). This comparison is equivalent to checking both sides of the Chapman-Kolmogorov equality (Eq. 3.3) when  $a = 1$ . Of note, error is not proportional to joint probabilities. This suggests that the source of the error has motif-dependent structure (on the contrary, errors from undersampling of probability distributions or stationary Gaussian heterogeneity in transition structure would predict a probability-proportional error).

We next investigated the structure of spatial heterogeneity, specifically how motif usage (marginal probability) and self-transition (joint probability of adjacent labels being the same motif) are dependent on physical space. To be precise, we found that the motif usage probability is conditioned on location  $p(S_t = k|Coor = (x, y))$  (examples shown in Fig. 3.5(d)), as well as on the motif self-transition probability  $p(S_{t+1} = k|Coor = (x, y), S_t = k)$  (Fig. 3.5 (e)). As a reference, an image of the arena floor is shown in Fig. 3.5 (c), and a heatmap of rats’ overall placement across the arena is offered in Fig. 3.5 (f).

### 3.5 Motif usage and assembly are experimentally significant

In previous experimental investigations using the restrainer paradigm (the experimental setup in the current study), prosocial behaviors between rats were studied[2, 3, 4, 28]. In short, if the free rat in the arena opens the restrainer door and releases the trapped rat, this is determined to be a prosocial act (validity of this claim was demonstrated in

[4]). Further, in these investigations, a free rat is designated an “opener” if it opens from the trapped rat three times in a row among 12 testing sessions. We can likewise classify the sessions used in the current study into those of openers (N=63) and those of non-openers (N=105). Importantly, rats were classified into the two categories in an analysis independent of the current one.

Next, we asked if rats of different levels of prosociality have diverging behavioral motif usage, transition dynamics, and spatial heterogeneities. In terms of motif usage, we again ranked the motifs by overall usage, with motif #1 being the mostly frequently used motif overall. We then divided the sessions into those of openers and those of non-openers, and compared the usage between groups for each session. We used Student’s t test for significance and Bonferroni correction to counter multiple comparison error. Among 1-sec motifs, four are used significantly differently between the two groups (motifs #1 and #7,  $p < 0.01$ ; motifs #6 and #27,  $p < 0.05$ ; after Bonferroni correction; Fig. 3.6 (a)). Similarly, we found that openers and non-openers have different transition dynamics (Fig. 3.6 (b)-(e)).

### 3.6 Syntactic constraints on motif assembly

Without constraints, motifs on a lower scale can theoretically be assembled into a large variety of sequences. For instance, the 33 1-sec motifs can be assembled into roughly  $4 \times 10^7$  different 5-sec long sequence and exponentially more sequences for longer intervals. However, the syntax of motif assembly will likely strongly constrain the patterns of combinations allowed. We here investigated these constraints by identifying “phrases” – sequences of motifs that are stereotyped and repeatedly used. Towards this end, layered hidden Markov models (LHMM) were used to discover whether such combinations exist.

The structure of an LHMM has been described in the Methods section. In short, we first built and fitted an HMM for 1-sec motifs (the model is described by  $\{\mathbf{A}_1, \boldsymbol{\pi}_1, \boldsymbol{\mu}_1, \boldsymbol{\Sigma}_1\}$ ). We then used the model to classify the 1-sec segments into the motifs, generating a label vector  $\mathbf{K}_1$  of size  $N$ . We built a matrix  $\tilde{\mathbf{K}}_1$  of size  $N$ -by- $D$ , where each column is the mean vector of the corresponding label in  $\mathbf{K}_1$  (i.e.  $\tilde{\mathbf{K}}_{1n} = \boldsymbol{\mu}_{1,k}$ , where  $k = \mathbf{K}_{1n}$ ). We then used the segmentation-decomposition procedure and segmented  $\tilde{\mathbf{K}}_1$  into segments of size  $\tau$ , creating a tensor of size  $\frac{N}{\tau}$ -by- $D$ -by- $\tau$ . This tensor was used as the input for the higher-layer HMM. A diagram of this process is offered in Fig. 3.7 (a).

We evaluated whether behavioral phrases exist, and, if so, how they are organized using the same model evaluation approach shown in Fig. 3.1. In short, we built a Gaussian model (GM), which does not assume the existence of distinct “phrases”; a Gaussian mixture model (GMM), which assumes existence of phrases; and a Gaussian-emission HMM

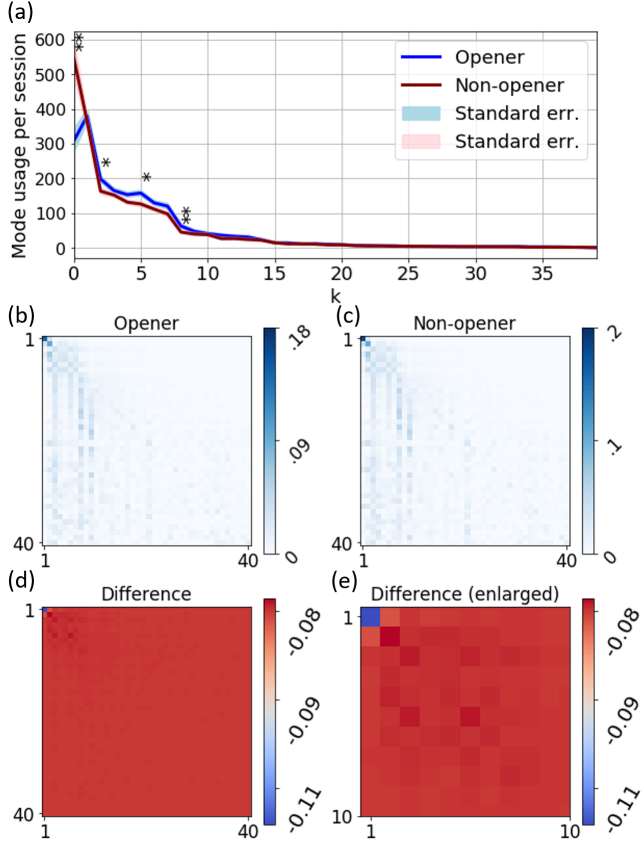


Figure 3.6: Motif usage and assembly are governed by different probability distributions between opener rats and non-opener rats. (a) Marginal probabilities of motifs on 1-sec timescale diverge between opener rats and non-opener rats. \* shows  $p < 0.00125$ ; \*\*  $p < 0.00025$ . Bonferroni corrected for multiple comparison. (b) Transition matrix for opener rats. (c) Transition matrix for non-opener rats. (d) Difference between transition matrices. (e) Enlarged view of a portion of (d).

(which we simply refer to as HMM), which assumes existence of phrases and Markov transition between said phrases. The models were then evaluated on randomly held-out data (30% of total dataset), using log likelihood as the metric. The results, shown in Fig. 3.7 (b), suggest that HMM outperforms both GMM and GM. These results indicate that there are stereotyped 5-sec long combinations of 1-sec long motifs, and that the transition between these combinations has history dependence.

### 3.6.1 Motifs converge with increasing timescale following strong constraints

Next, we investigated the relationship between motifs at different timescales. Note that the dimensionality reduction from lower timescale to higher timescale is remarkable – if the motif usage probabilities are uniform, 33 1-sec motifs could form almost  $4 \times 10^7$  different 5-sec long sequences, instead of the 25 observed. This suggests that there are strict constraints on the transition dynamics (e.g. the conditional probability  $p(S_{t+1}|S_t)$ ) at a low timescale (only a few 5-sec long sequences are dominantly likely) and/or the motif usage probabilities (e.g. the marginal probability  $p(S_t)$ ).

To test whether the marginal probabilities ( $p(S_t)$ ) are significantly non-uniform, we compared the distributions against uniform probability distributions at different timescales, using the Kullback-Leibler divergence ( $D_{KL}$ ) as metric. Specifically, for each marginal probability vector  $\mathbf{P}_m$  that the model  $HMM_m$  gives, we generated a same-size vector  $\hat{\mathbf{P}}_m$  where all elements are equal and sum to unity. Note that both vectors are of size  $K_m$ , since each motif in the model has its marginal probability and there are  $K$  motifs in each model. Also note that the model used for different timescales have different  $K$ , therefore each model has its own  $K$ , denoted as  $K_m$ . To control for differences caused by vector size, we also generated vectors of size  $K_m$  where each probability is randomly drawn from a uniform distribution and then normalized such that the vector sums to unity. We denote these vectors  $\hat{\mathbf{P}}_m$ . Kullback-Leibler divergence is computed as

$$D_{KL}(\mathbf{P}_m || \hat{\mathbf{P}}_m) = \sum_k^{K_m} (\mathbf{P}_m)_k \log \frac{(\mathbf{P}_m)_k}{(\hat{\mathbf{P}}_m)_k}.$$

Results suggest that observed marginal probabilities at low timescales are widely different from uniform, supporting the hypothesis that lower-timescales have constrained marginal probabilities (Fig. 3.7 (d)). This would suggest that lower-timescale motif usage is subject to more constraints than higher-timescale motif usage, which can be explained by the fact that biomechanical constraints are more prominent at lower timescales than higher ones.

Suiting conditional probability (i.e. the transition matrix) could restore uniformity in the joint probability distributions

despite highly constrained marginals. To discover if that is the case, we computed the joint probability structures for 2, 3, 4 adjacent motifs. These structures give a probability for every possible combination of motifs of length 2, 3, and 4, and therefore are in the shape of  $K^2$  squares,  $K^3$  cubes, and  $K^4$  tesseracts, respectively. For ease of illustration, we show the 2-dimensional case in Fig. 3.7 (c).

### 4 Discussion

In the current study, we used an innovative, multi-scale approach to uncover the vocabulary and syntax of rat locomotor behaviors. In the analogy of locomotion as a language, we mapped out “phonemes” (short, basic level motifs) as well as “expressions” (long, large-scale motifs), and the syntactical rules that govern their assembly into the locomotor trajectories that we observe. Importantly, we challenge the long-held implicit assumption in animal behavior modeling that behavioral sequences can be adequately described with motifs on one scale. Instead, our results suggest that locomotor trajectories are the combined outcome of several stochastic processes that run in parallel on different spatial-temporal scales. Behavior “sequence” becomes a misnomer, because behavior cannot simply be decomposed into one behavior after another. Instead, an organism is performing multiple behaviors on multiple scales at any time point. A complete description of his behaviors must include behavioral motifs and how motifs are assembled on each of these scales. The multi-scale dynamics of behavior has implications for investigations of neural circuits generative of behaviors. Circuits are not merely generating motor patterns at one scale and receiving modulations from long-timescale processes. Instead, circuits are simultaneously supporting patterns on different scales. How slow dynamics influence fast dynamics in behaviors, or vice versa, may reflect how slow modulation affects circuit activity in the nervous system. In addition, our approach produces a reduced representation of rodent behavior that can be used towards building more mechanistic models (e.g. [26]).

To capture multi-scale behavioral dynamics, we developed and employed computational methods that are well-suited for multi-scale modeling. We used a segmentation-decomposition procedure and multiple parallel hidden Markov models (HMM) to overcome existing methods’ single-scale limit. The segmentation-decomposition procedure is an important step towards efficiently modeling supra-second dynamics in behavior. As explained previously, a primary challenge in modeling long-timescale behavior is that larger-scale motifs contain more variance than small-scale motifs. Consequently, large motifs dominate over small motifs in dimensionality reduction. On the other hand, fast dynamics in observed behaviors tend to dominate over slow dynamics in models of time series. The segmentation-decomposition procedure circumvented the issue of larger-scale motifs dominating over small-scale motifs by imposing

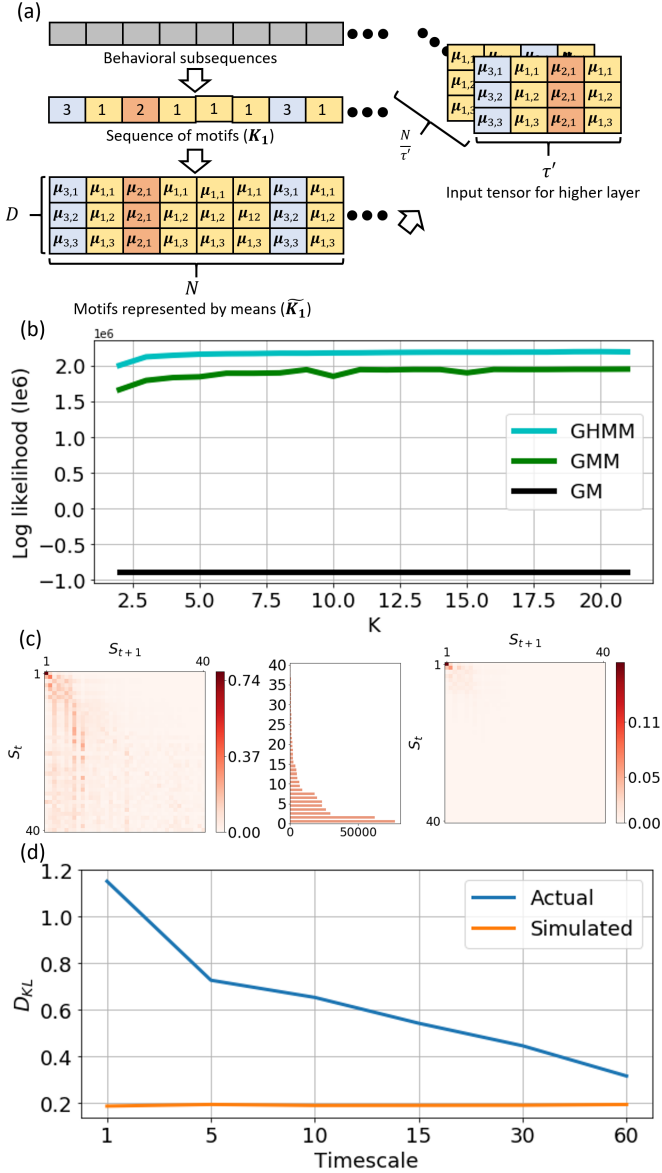


Figure 3.7: Transition matrix further constrains probability of transitions. (a). Diagram illustrating how output from a lower level HMM is processed into input for a higher layer. (b). Comparison of model performance on the higher layer HMM based on maximum likelihood. HMM is favored. (c) Left panel: Transition probability structure ( $p(S_{t+1}|S_t)$ ) is not uniform. Mid panel: marginal probability of motifs ( $p(S_t)$ ) is not uniform. Right panel: Joint probability of adjacent motifs ( $p(S_{t+1}, S_t)$ ) is further lopsided. (d) Kullback-Leibler divergence between observed marginal probabilities and uniform probabilities decreases across timescales.



strong constraints on the motif size that can be discovered. Performing dimensionality reduction at different scales allows the relevant features of each scale to be captured simultaneously. As a result, the same locomotor trajectory is segmented and decomposed at different levels of granularity in parallel. This approach cannot be substituted with modified versions of HMM (e.g. autoregressive HMM, layered HMM). This is because these models can capture large scale assembly rules of small scale motifs, but not the morphology of the large scale motifs. Our results also offer a detailed look at advantages and limitations of applying HMMs (and Markov process models) to supra-second behavioral data. On one hand we successfully discovered motifs related to prosociality in rats, demonstrating experimental significance of the behavioral vocabulary that we discovered. On the other hand, we found strong heterogeneity in motif usage and transition that is not captured by homogeneous Markov processes. Importantly, such heterogeneity is space-dependent, and therefore can hardly be captured by adding time-dependent hidden variables to the model.

While our approach imposes significantly less constraint on the structure of slow dynamics than competing approaches (e.g. ARHMM), there are still limitations. First, we relied on PCA for dimensionality reduction of locomotor trajectories. Since the success of PCA relies on linear separability of trajectories in the data space, the length of trajectory segments is limited. In our case, one minute appears to be the upper limit for a 5-component PCA-based decomposition. This issue could be circumvented by incorporating trajectory-informed kernels in the decomposition process[25]. Second, we note that our model does not take feedforward-feedback between slow dynamics and fast dynamics into consideration. Including such connections in the model would lead to exponential growth of free parameters in the model and require much larger datasets to fit. Simplifications of slow dynamics may help trim down parameters and prevent overfitting.

As biomechanical systems, physical bodies of rats have a high degree of freedom. Looked at individually, the joints, limbs, muscles of them can contract, bend, twist, relax in seemingly uncountable ways. The same can be said for locomotor trajectories – as moving objects, rats could move in trajectories that are straight, twisty, circular and so on. However, we found that the observed trajectories are highly constrained. First, high-dimensional trajectories are effectively represented by linear combinations of 5 principle components. In other words, 5 features on each timescale can adequately describe the range of motion that rats undertake. Second, trajectories on each level are composed of at most dozens of motifs. This suggests a limited behavioral repertoire. Finally, very few out of the numerous combinations of motifs are possible and actually observed. On one hand, these findings paint a promising picture for using automated approaches to parse out behavioral observations, since the possible behaviors are limited to a relatively small repertoire. On the other hand, the findings offer insights

into the dynamics of motor-pattern-generating neural circuits. Viewed as dynamical systems, these circuits must have limited stable states that they oscillate between.

There are limitations and obvious next steps that are not addressed in the current study. First of all, there are few metrics that can guide the granularity selection for the segmentation-decomposition procedure. To err on the side of redundancy, we performed the procedure on many levels of granularity, which may not have been necessary. A possible solution is to segment trajectories at increasing intervals and compare at which intervals HMMs fit best. Second, the heterogeneity discovered can be and should be incorporated back into the hidden Markov models. The transition matrix will be a function of external factors (or, as in the case of autoregressive models, the Markov process itself), rather than being time-invariant. Prominent candidates for external modulation of transition dynamics are, as we showed, location in the physical space, and the motif being used at other timescales. The modulations make intuitive sense: an organism makes behavioral decisions based on external input, and what it’s higher-level “motivation” is.

Despite the widespread use of behavioral assays involving rat locomotion, the design and interpretation of these assays does not stem from an understanding of the underlying organizational dynamics. Discovering the building blocks and rules of rat behaviors is central to correctly identifying the neural substrates that produce behaviors. By finally knowing what are the stereotyped behaviors that animals perform, and under what circumstances they are performed, we move closer to mechanistic explanations of behaviors. In addition, since our approach captures dynamics at different scales simultaneously, it forms an important framework for studying state-dependent behaviors.

## References

- [1] Mehdi Azzouzi and Ian T Nabney. Modelling financial time series with switching state space models. In *Computational Intelligence for Financial Engineering, 1999.(CIFER) Proceedings of the IEEE/IAFE 1999 Conference on*, pages 240–249. IEEE, 1999.
- [2] Inbal Ben-Ami Bartal, Jean Decety, and Peggy Mason. Empathy and pro-social behavior in rats. *Science*, 334(6061):1427–1430, 2011.
- [3] Inbal Ben-Ami Bartal, David A Rodgers, Maria Sol Bernardez Sarria, Jean Decety, and Peggy Mason. Pro-social behavior in rats is modulated by social experience. *Elife*, 3:e01385, 2014.
- [4] Inbal Ben-Ami Bartal, Haozhe Shan, Nora MR Molasky, Teresa M Murray, Jasper Z Williams, Jean Decety, and Peggy Mason. Anxiolytic treatment impairs helping behavior in rats. *Frontiers in psychology*, 7, 2016.



- [5] Leonard E Baum. An inequality and associated maximization technique in statistical estimation for probabilistic functions of markov process. *Inequalities*, 3:1–8, 1972.
- [6] Gordon J Berman, Daniel M Choi, William Bialek, and Joshua W Shaevitz. Mapping the stereotyped behaviour of freely moving fruit flies. *Journal of The Royal Society Interface*, 11(99):20140672, 2014.
- [7] Christopher M Bishop. *Pattern recognition and machine learning*. springer, 2006.
- [8] Robert J Blanchard, Kenneth Fukunaga, D Caroline Blanchard, and Michael J Kelley. Conspecific aggression in the laboratory rat. *Journal of comparative and physiological psychology*, 89(10):1204, 1975.
- [9] André EX Brown, Eviatar I Yemini, Laura J Grundy, Tadas Jucikas, and William R Schafer. A dictionary of behavioral motifs reveals clusters of genes affecting *caenorhabditis elegans* locomotion. *Proceedings of the National Academy of Sciences*, 110(2):791–796, 2013.
- [10] Hung Hai Bui, Svetha Venkatesh, and Geoff West. Policy recognition in the abstract hidden markov model. *Journal of Artificial Intelligence Research*, 17:451–499, 2002.
- [11] Michael J Detke, Michael Rickels, and Irwin Lucki. Active behaviors in the rat forced swimming test differentially produced by serotonergic and noradrenergic antidepressants. *Psychopharmacology*, 121(1):66–72, 1995.
- [12] G David Forney. The viterbi algorithm. *Proceedings of the IEEE*, 61(3):268–278, 1973.
- [13] Crispin Gardiner. Stochastic methods. *Springer Series in Synergetics (Springer-Verlag, Berlin, 2009)*, 1985.
- [14] Tiago V Gehring, Gediminas Luksys, Carmen Sandi, and Eleni Vasilaki. Detailed classification of swimming paths in the morris water maze: multiple strategies within one trial. *Scientific reports*, 5, 2015.
- [15] Robert E Kass and Larry Wasserman. A reference bayesian test for nested hypotheses and its relationship to the schwarz criterion. *Journal of the american statistical association*, 90(431):928–934, 1995.
- [16] Richard J Katz, Kevin A Roth, and Bernard J Carroll. Acute and chronic stress effects on open field activity in the rat: implications for a model of depression. *Neuroscience & Biobehavioral Reviews*, 5(2):247–251, 1981.
- [17] Geoffrey A Lambert, George Mallos, and Alessandro S Zagami. Von frey’s hairs—a review of their technology and use—a novel automated von frey device for improved testing for hyperalgesia. *Journal of neuroscience methods*, 177(2):420–426, 2009.
- [18] David JC MacKay. *Information theory, inference and learning algorithms*. Cambridge university press, 2003.
- [19] Todd K Moon. The expectation-maximization algorithm. *IEEE Signal processing magazine*, 13(6):47–60, 1996.
- [20] Richard Morris. Developments of a water-maze procedure for studying spatial learning in the rat. *Journal of neuroscience methods*, 11(1):47–60, 1984.
- [21] Nam Thanh Nguyen, Dinh Q Phung, Svetha Venkatesh, and Hung Bui. Learning and detecting activities from movement trajectories using the hierarchical hidden markov model. In *Computer Vision and Pattern Recognition, 2005. CVPR 2005. IEEE Computer Society Conference on*, volume 2, pages 955–960. IEEE, 2005.
- [22] Lucas PJJ Noldus, Andrew J Spink, and Ruud AJ Tegelenbosch. Ethovision: a versatile video tracking system for automation of behavioral experiments. *Behavior Research Methods*, 33(3):398–414, 2001.
- [23] Cort A Pedersen and Arthur J Prange. Oxytocin and mothering behavior in the rat. *Pharmacology & therapeutics*, 28(3):287–302, 1985.
- [24] Tomasz Schneider and Ryszard Przewlocki. Behavioral alterations in rats prenatally exposed to valproic acid: animal model of autism. *Neuropsychopharmacology*, 30(1):80, 2005.
- [25] Bernhard Schölkopf, Alexander Smola, and Klaus-Robert Müller. Kernel principal component analysis. In *International Conference on Artificial Neural Networks*, pages 583–588. Springer, 1997.
- [26] Monika Scholz, Aaron R Dinner, Erel Levine, and David Biron. Stochastic feeding dynamics arise from the need for information and energy. *Proceedings of the National Academy of Sciences*, page 201703958, 2017.
- [27] Richard Serfozo. *Basics of applied stochastic processes*. Springer Science & Business Media, 2009.
- [28] Haozhe Shan, Inbal Ben-Ami Bartal, and Peggy Mason. A rodent model of social rejection. *bioRxiv*, page 066993, 2016.
- [29] Dallas Treit and M Fundytus. Thigmotaxis as a test for anxiolytic activity in rats. *Pharmacology Biochemistry and Behavior*, 31(4):959–962, 1988.
- [30] Alexander Waibel, Toshiyuki Hanazawa, Geoffrey Hinton, Kiyohiro Shikano, and K Lang. Phoneme recognition: neural networks vs. hidden markov models vs. hidden markov models. In *Acoustics, Speech, and Signal Processing, 1988. ICASSP-88., 1988 International Conference on*, pages 107–110. IEEE, 1988.

- [31] Roger N Walsh and Robert A Cummins. The open-field test: A critical review. *Psychological bulletin*, 83(3):482, 1976.
- [32] Christian Wellekens. Explicit time correlation in hidden markov models for speech recognition. In *Acoustics, Speech, and Signal Processing, IEEE International Conference on ICASSP'87.*, volume 12, pages 384–386. IEEE, 1987.
- [33] Ian Q Whishaw and Bryan Kolb. *The behavior of the laboratory rat: a handbook with tests*. Oxford University Press, 2004.
- [34] Alexander B Wiltschko, Matthew J Johnson, Giuliano Iurilli, Ralph E Peterson, Jesse M Katon, Stan L Pashkovski, Victoria E Abaira, Ryan P Adams, and Sandeep Robert Datta. Mapping sub-second structure in mouse behavior. *Neuron*, 88(6):1121–1135, 2015.
- [35] Daniel M Wolpert and Zoubin Ghahramani. Computational principles of movement neuroscience. *Nature neuroscience*, 3(11s):1212, 2000.

## 5 Supplementary materials

### 5.1 PCA decomposition of trajectory segments

The extracted eigen-trajectories suggest distinct features at different timescales (Fig. 5.1). At a short timescale (here, 1-second-long segments), the dominant elementary trajectories are uniform motions (constant speed, fixed direction); less dominant eigen-trajectories, however, show oscillations in both the X-time plane (suggesting back-and-forth motion) and the Y-time plane (suggesting swiveling motion).

### 5.2 Fitting hidden Markov models (HMM) to behavioral sequences

Hidden Markov models (HMM) are commonly used for modeling time series (Bishop, 2006). While its application to animal behavior data is relatively new, HMM and its variants have long been applied to human behavior data, such as human speech recognition and synthesis (Huang et al., 1990; Mqasuko et al., 1996) and human handwriting recognition (Hu et al., 1996). As discussed in the main text, the fundamental assumptions of HMM-based modeling is that the time series is composed of repeated, stereotyped modes, and that mode selection is Markovian. Given stereotyped behaviors that have been discovered through human observation, it is reasonable to assume the existence of other such modes in animal behavior. In addition, HMMs have

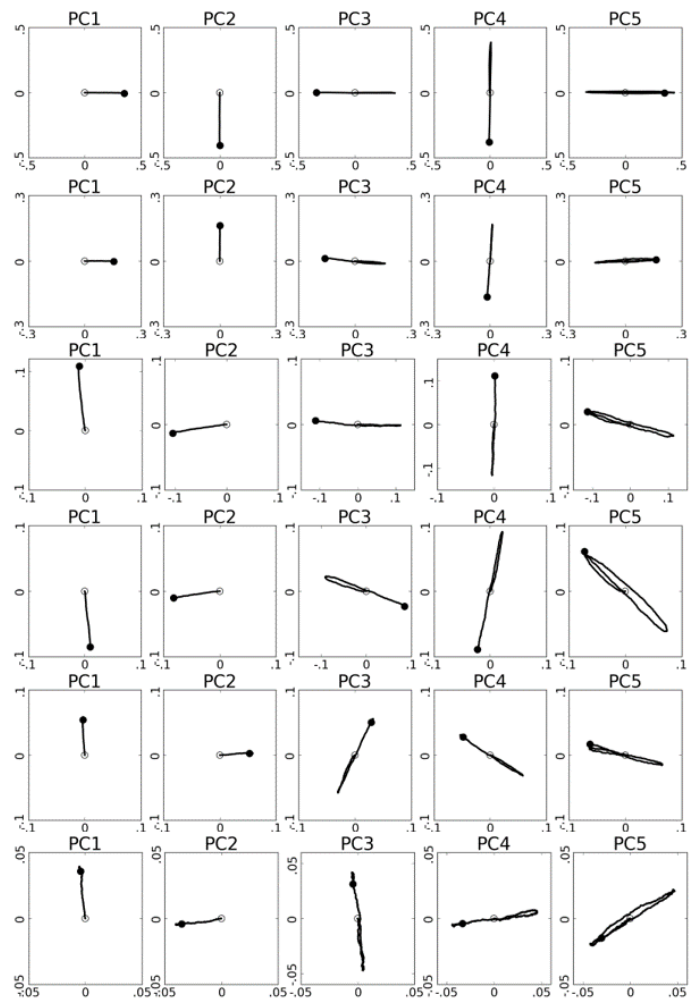


Figure 5.1: Top to bottom: principle components of segments created at 1, 5, 10, 15, 30, and 100 second intervals. Empty markers mark starting points and filled markers stopping points. X-Y axes are dimensions in physical space (arbitrary length unit).

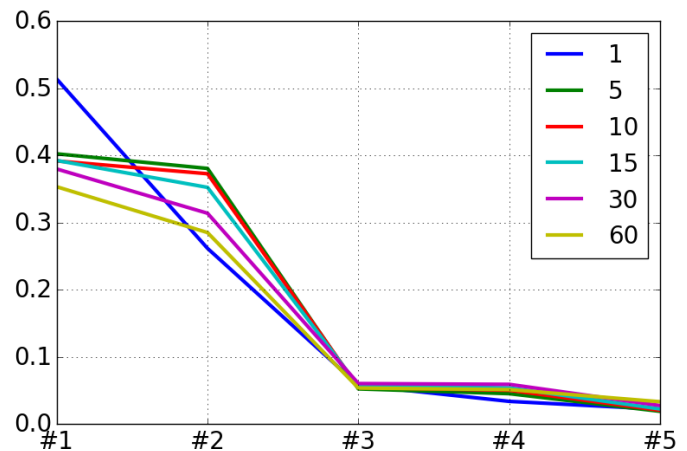


Figure 5.2: Principle component analysis reveals highly manifold structure of locomotor trajectories.

several other advantageous features. First, mixture models are special cases of HMMs (where  $p(S_{t+1}|S_t) = p(S_{t+1})$ ). This means that if actual behavioral mode selection has no history dependence, HMM would not force history dependence on the model. Second, HMMs have good time-warp invariance (Bishop, 2006) – that is, if the behavioral motifs are warped across time and/or space, they can still be well recognized and correctly classified. This is particularly useful for locomotor trajectories, which are prone to warping. Finally, classifying trajectory segments into identified motifs with HMMs takes trajectory history into account, unlike straightforward clustering algorithms (e.g. K-means in Gehring et al., 2015).

### 5.3 Lower bound for Hamming loss

Hamming loss between two same-sized vectors of labels in the same label space is defined as the Hamming distance between the labels divided by the sequence size  $N$ . Hamming distance between two sequences is the number of minimum edits required to equate the two vectors. Formally,

$$\mathcal{L}^H(\mathbf{X}, \mathbf{Y}) = \frac{\mathcal{D}^H(\mathbf{X}, \mathbf{Y})}{N}.$$

In the context of multi-label classification, the Hamming distance between the vector of correct labels (denoted as  $\mathbf{S}$ ) and the vector of inferred labels (denoted as  $\hat{\mathbf{S}}$ ) is the number of incorrectly inferred labels. Here we offer an informal proof of the lower bound for Hamming loss in multi-label classification, given the probability distribution of true labels and inferred labels.

**Proof** Given two same-sized vectors  $\mathbf{S}$  and  $\hat{\mathbf{S}}$  of size  $N$  where each value takes on a label from  $1, 2, 3, \dots, K$ , a set we denote as  $\mathcal{K}$ . The Hamming loss between the two vectors has lower bound  $\frac{1}{2} \sum_k^K |p(S_t = k) - p(\hat{S}_t = k)|$  at the large  $N$  limit.

At the large  $N$  limit, we have  $N_{S_t=k} = Np(S_t = k)$  and likewise  $N_{\hat{S}_t=k} = Np(\hat{S}_t = k)$ .

To minimize  $\mathcal{D}^H(\mathbf{X}, \mathbf{Y})$ , we maximize  $N_{S_t=\hat{S}_t=k}$  for all  $k$ . It is obvious that  $N_{S_t=\hat{S}_t=k} = \min(N_{S_t=k}, N_{\hat{S}_t=k})$  is the loss-minimizing classification. We divide  $\mathcal{K}$  into three subsets,  $\mathcal{K}_E$  where  $\forall k \in \mathcal{K}_E : N_{S_t=k} = N_{\hat{S}_t=k}$ ,  $\mathcal{K}_L$  where  $\forall k \in \mathcal{K}_L : N_{S_t=k} > N_{\hat{S}_t=k}$ , and  $\mathcal{K}_S$  where  $\forall k \in \mathcal{K}_S : N_{S_t=k} < N_{\hat{S}_t=k}$ . Since  $\sum_k N_{S_t=k} = \sum_k N_{\hat{S}_t=k} = N$ ,

$$\sum_{k \in \mathcal{K}_L} (N_{S_t=k} - N_{\hat{S}_t=k}) = \sum_{k \in \mathcal{K}_S} (N_{\hat{S}_t=k} - N_{S_t=k}) \leq \mathcal{D}^H(\mathbf{S}, \hat{\mathbf{S}}).$$

We thus obtain

$$\begin{aligned} \mathcal{D}^H(\mathbf{S}, \hat{\mathbf{S}}) &\geq \sum_{k \in \mathcal{K}_L} (N_{S_t=k} - N_{\hat{S}_t=k}) \\ &= \sum_{k \in \mathcal{K}_S} (N_{\hat{S}_t=k} - N_{S_t=k}) \\ &= N \sum_{k \in \mathcal{K}_L} |p(S_t = k) - p(\hat{S}_t = k)| \\ &= N \sum_{k \in \mathcal{K}_S} |p(S_t = k) - p(\hat{S}_t = k)|. \end{aligned}$$

Given  $N \sum_{k \in \mathcal{K}_E} |p(S_t = k) - p(\hat{S}_t = k)| = 0$ , we have

$$\begin{aligned} \mathcal{D}^H(\mathbf{S}, \hat{\mathbf{S}}) &\geq \frac{1}{2} \left[ N \sum_{k \in \mathcal{K}_L} |p(S_t = k) - p(\hat{S}_t = k)| \right. \\ &\quad \left. + N \sum_{k \in \mathcal{K}_S} |p(S_t = k) - p(\hat{S}_t = k)| \right. \\ &\quad \left. + N \sum_{k \in \mathcal{K}_E} |p(S_t = k) - p(\hat{S}_t = k)| \right] \\ &= \frac{1}{2} N \sum_k |p(S_t = k) - p(\hat{S}_t = k)|. \end{aligned}$$

Therefore,

$$\mathcal{L}^H(\mathbf{S}, \hat{\mathbf{S}}) \geq \frac{\mathcal{D}^H(\mathbf{S}, \hat{\mathbf{S}})}{N} = \frac{1}{2} \sum_k |p(S_t = k) - p(\hat{S}_t = k)| \blacksquare.$$

In the main text, we used joint probability distributions of adjacent labels instead of marginal distributions of individual labels. The only difference is that the set of labels  $\mathcal{K}$  is of size  $K^2$  and the proof follows.

## 6 Acknowledgement and Information

The authors would like to thank Monika Scholz and Jonathan Pillow for helpful discussions on modeling; Nora Molasky, Maria Sol Bernardez Sarria and Tess Murray for help with data collection. The authors declare no conflicting interests. The work was supported by the Earl Franklin Research Fellowship (HZS).